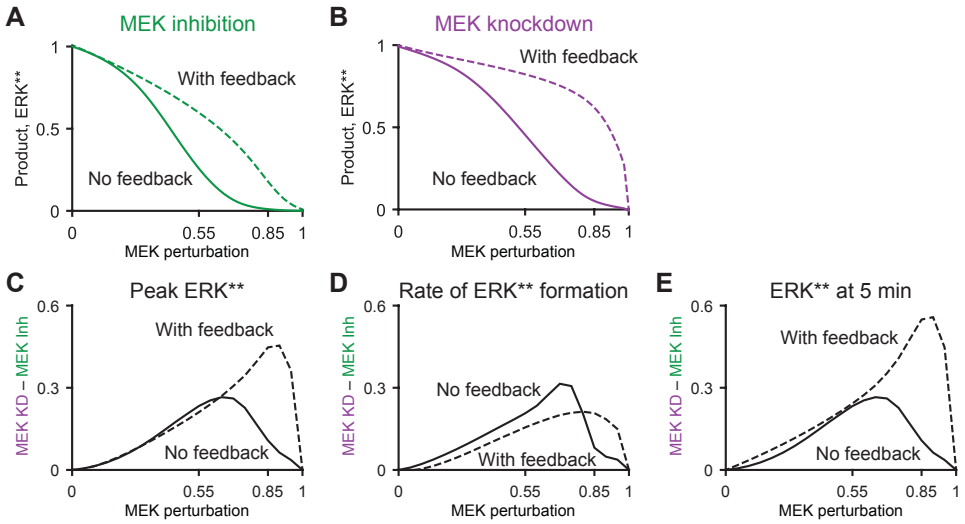


**Figure S1. Related to Figure 2.** Robust enhancement of knockdown-inhibitor discrepancy in the presence of Raf –| ERK feedback. (*A* and *B*) MEK knockdown is disproportionately affected by Raf –| ERK feedback. Simulations from Figures 2E and 2F are replotted to compare (*A*) MEK inhibition and (*B*) MEK knockdown with (dashed) or without (solid) Raf –| ERK feedback. (*C* to *E*) Enhanced knockdown-inhibitor discrepancy at strong MEK perturbations is not dependent on the choice of ERK activity metric. The simulations of Figure 2 are replotted with (dashed) or without (solid) Raf –| ERK feedback, where ERK signaling is measured as a function of (*C*) peak ERK activity, (*D*) peak rate of ERK activation, or (*E*) ERK activity at 5 minutes when the step activation of RasGTP stops.

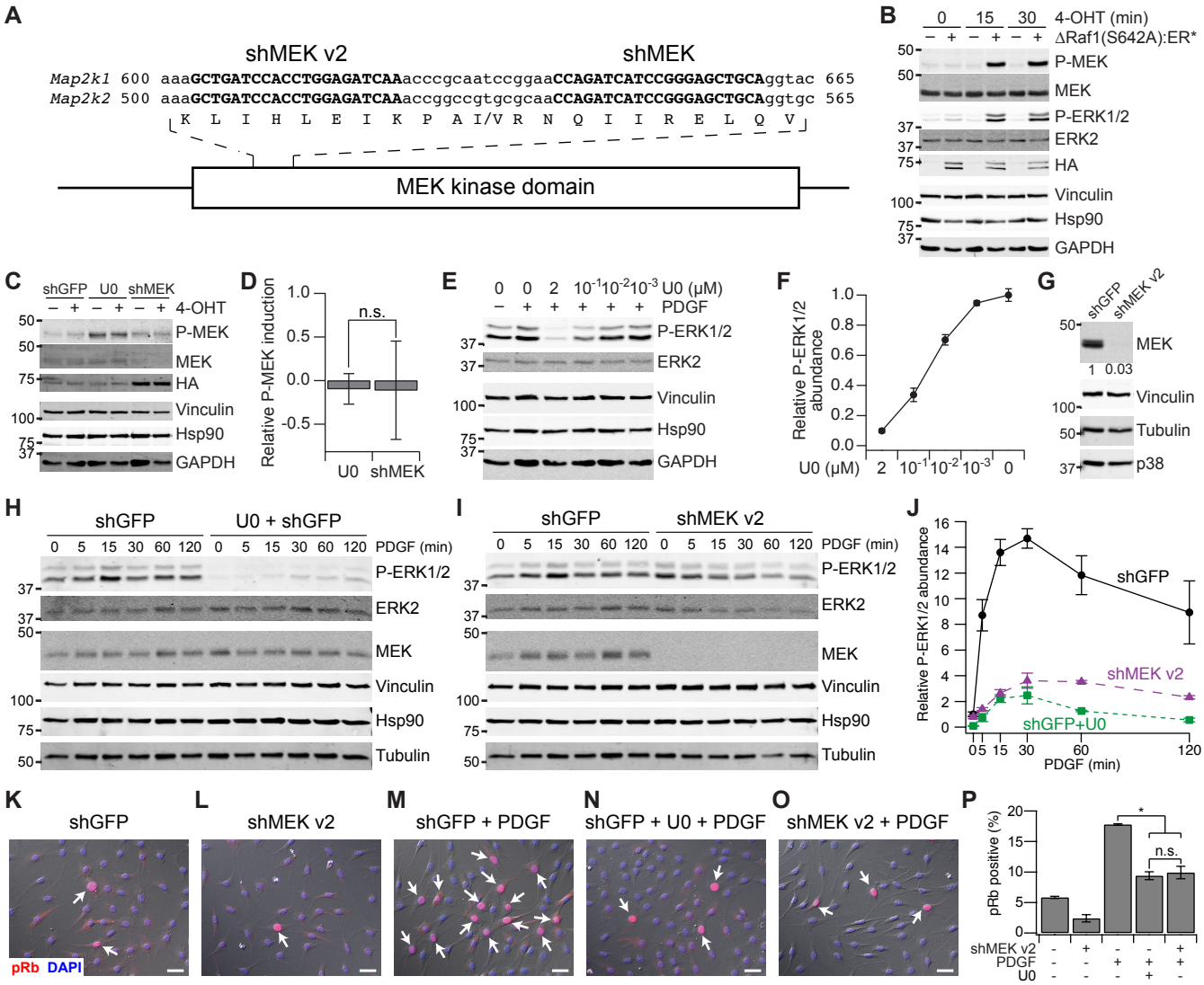


**Figure S2. Related to Figure 3.** Perturbation of PDGF- and hormone-stimulated activation of MAPK signaling.
(*A*) Design of two shRNAs (shMEK and shMEK v2) targeting the *Map2k1* and *Map2k2* isoforms of murine MEK.
(*B*) Validation of hormone-induced, feedback-resistant Raf1. 293T cells were transfected with HA-ΔRaf1(S642A):ER*, stimulated with 100 nM 4-hydroxytamoxifen (4-OHT), lysed, and immunoblotted for phosphorylated MEK (P-MEK), phosphorylated ERK1/2 (P-ERK1/2), and HA tag with total MEK, total ERK2, vinculin, Hsp90, and GAPDH used as loading controls.
(*C* and *D*) 4-OHT-induced MEK phosphorylation is blocked by 2 μM U0126 (U0) and shMEK. NIH 3T3 cells stably expressing HA-ΔRaf1(S642A):ER* were pretreated with 2 μM U0 or 0.1% DMSO, stimulated with 100 nM 4-OHT for 15 minutes, lysed, and immunoblotted for P-MEK, total MEK, and HA tag with vinculin, Hsp90, and GAPDH used as loading controls. In (*D*), relative 4-OHT-induced P-MEK is shown as the mean ± s.e.m. of four independent experiments.
(*E* and *F*) Dose-dependent inhibition of PDGF-induced P-ERK in NIH 3T3 cells stably expressing HA-ΔRaf1(S642A):ER*. Cells were pretreated with the indicated concentration of U0, stimulated with 1 ng/ml PDGF for 5 min, lysed and immunoblotted for P-ERK1/2 with total ERK2, vinculin, Hsp90, and GAPDH used as loading controls. In (*F*), relative PDGF-induced P-ERK1/2 is shown as the mean ± s.e.m. of three independent experiments.
(*G*) Knockdown of total MEK with shMEK v2. NIH 3T3 cells were transduced with the indicated lentiviruses, lysed, and immunoblotted for endogenous MEK with vinculin, tubulin, and p38 used as loading controls.
(*H* and *I*) PDGF-stimulated ERK phosphorylation is perturbed by U0 and shMEK v2. Cells were pretreated with 2 μM U0 or carrier, stimulated with 1 ng/ml PDGF for the indicated time points, lysed, and immunoblotted for phosphorylated ERK1/2 (P-ERK1/2) and MEK with total ERK2, vinculin, Hsp90, and tubulin used as loading controls.
(*J*) Replicated densitometry of the experiment in (*F* and *G*). Data are shown as the mean ± s.e.m. of four independent experiments.
(*K* to *O*) PDGF-stimulated proliferation is perturbed by U0 and shMEK v2. Cells were serum starved, pretreated with 2 μM U0 or carrier, stimulated with 1 ng/ml PDGF for 24 hr, and immunostained for hyperphosphorylated Rb (pRb, red) with DAPI (blue) used as a nuclear counterstain. Fluorescence images are shown overlaid on the accompanying DIC image. Scale bar is 20 μm.
(*P*) Frequency of pRb positive cells scored for the indicated conditions. Data are shown as the mean ± s.e.m. of three independent experiments. Asterisk indicates $p < 0.05$ by Welch's two-sided *t* test.

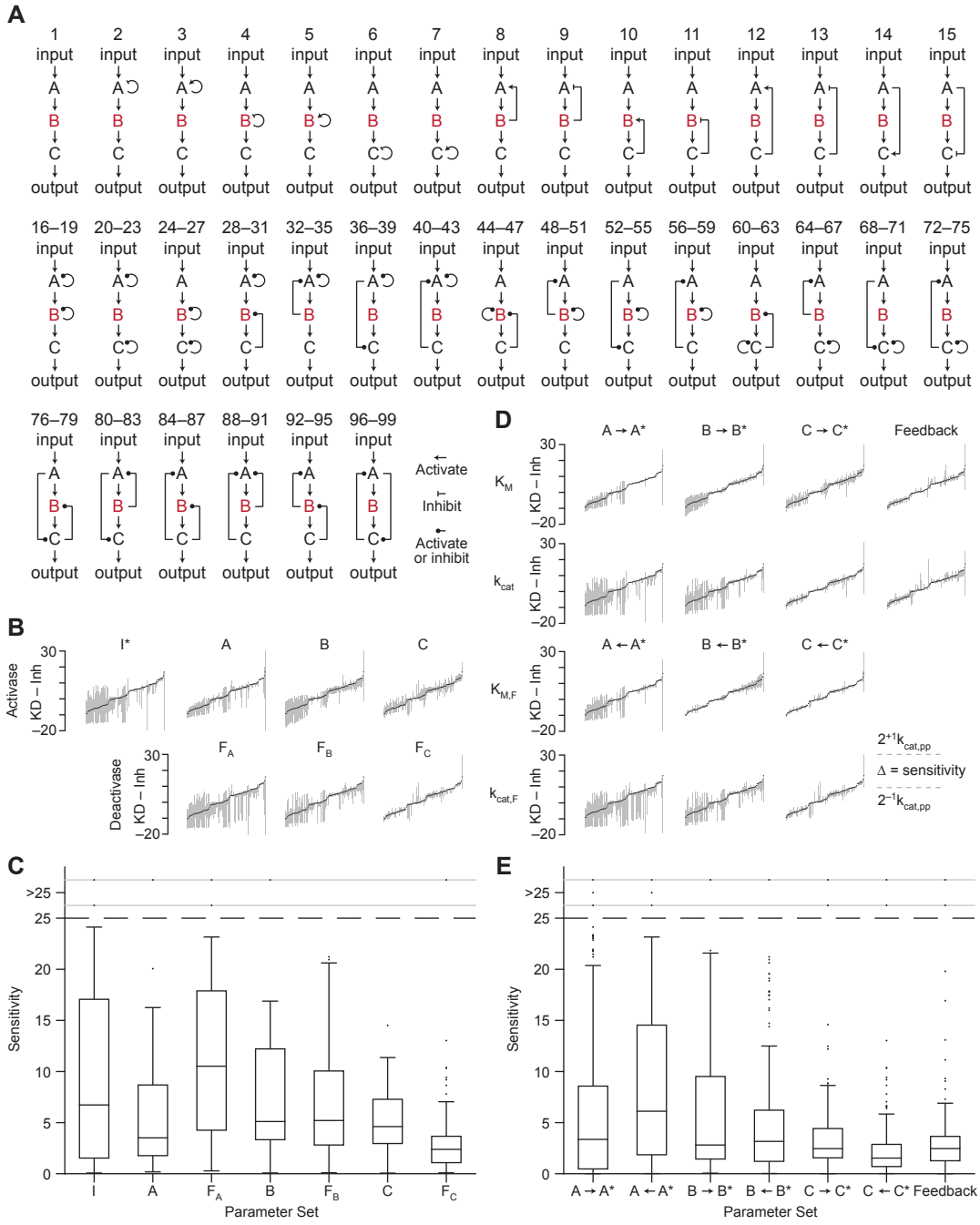


**Figure S3. Related to Figure 4.** Robust examination of knockdown-inhibitor discrepancy by exhaustive modeling of one- and two-edge network topologies in three-tiered enzyme cascades.

(*A*) Network topologies used for knockdown-inhibitor comparisons. Model parameters for the linear topology (Model 1) were optimized to yield nearly identical perturbations of active *C* (*C**) across the full perturbation range of *B* (red). One-edge topologies are enumerated in Models 2–15, and two-edge topologies are enumerated in Models 16–99.

(*B* and *C*) Sensitivity analysis of the integrated knockdown (KD)-inhibitor (Inh) discrepancy as a function of doubling or halving the initial conditions of the active input (*I**), the cascade activases (A, B, C), or the deactivases ($F_A$, $F_B$, $F_C$).

(*D* and *E*) Sensitivity analysis of the KD – Inh discrepancy as a function of doubling or halving the forward rate constants ($K_M$, $k_{cat}$) or the reverse rate constants ($K_{M,F}$, $k_{cat,F}$) for the indicated reactions (columns).

For (*B*) and (*D*), data are shown as the KD – Inh discrepancy of the optimized model (black) as in Figure 4A ± the range of doubling or halving the indicated model parameter (gray).

For (*C*) and (*E*), sensitivity is defined as the range of KD – Inh resulting from a doubling and halving of the indicated model parameter. Box-and-whisker plots show the median (line), 25$^{th}$-75$^{th}$ percentiles (box), 1.5× interquartile range (whiskers), and outliers (points) from perturbations aggregated across all 99 models.

**Table S1. Related to Figure 1.** Parameters in the three-tiered Michaelian cascade.

| Reaction | Initial conditions[†] | | Rate parameters[‡] | |
|---|---|---|---|---|
| $A \xrightarrow{I^*} A^*$ | $A = 1$ | $I^* = \begin{matrix} 1 & t = 0 - 5 \text{ min} \\ 0 & t > 5 \text{ min} \end{matrix}$ | $k_{cat,A} = 0.050 \text{ s}^{-1}$ | $K_{M,A} = 0.277$ |
| $A^* \xrightarrow{F_A} A$ | $A^* = 0$ | $F_A = 0.5$[§] | $k_{cat,FA} = 0.134 \text{ s}^{-1}$ | $K_{M,FA} = 0.136$ |
| $B \xrightarrow{A^*} B^*$ | $B = 1$ | $A^* = 0$ | $k_{cat,B} = 0.262 \text{ s}^{-1}$ | $K_{M,B} = 0.020$ |
| $B^* \xrightarrow{F_B} B$ | $B^* = 0$ | $F_B = 0.5$[§] | $k_{cat,FB} = 0.104 \text{ s}^{-1}$ | $K_{M,FB} = 0.223$ |
| $C \xrightarrow{B^*} C^*$ | $C = 1$ | $B^* = 0$ | $k_{cat,C} = 0.539 \text{ s}^{-1}$ | $K_{M,C} = 2.009$ |
| $C^* \xrightarrow{F_C} C$ | $C^* = 0$ | $F_C = 0.5$[§] | $k_{cat,FC} = 0.111 \text{ s}^{-1}$ | $K_{M,FC} = 0.221$ |
| $A^* \xrightarrow{C^*} A$[¶] | $A^* = 0$ | $C^* = 0$ | $k_{cat,feedback} = 2.77 \text{ s}^{-1}$ | $K_{M,feedback} = 0.054$ |

[†]Species concentrations are shown in arbitrary units.
[‡]Rate parameters were optimized so that knockdown and inhibition of *B* yielded the same inhibition of *C** across the full range of *B* perturbation in the linear cascade.
[§]Deactivating enzymes were kept constant throughout the simulations.
[¶]Reaction added to the *C* –| *A* feedback model.

**Table S2. Related to Figure 4.** Parameters in the three-tiered Michaelian cascade with regulatory elaborations.

| Reaction | Initial conditions† | | Rate parameters‡ | |
|---|---|---|---|---|
| $A \xrightarrow{I^*} A^*$ | $A = 1$ | $I^* = \begin{cases} 1 & t = 0 - 5 \text{ min} \\ 0 & t > 5 \text{ min} \end{cases}$ | $k_{cat,A} = 0.050 \text{ s}^{-1}$ | $K_{M,A} = 0.277$ |
| $A^* \xrightarrow{F_A} A$ | $A^* = 0$ | $F_A = 0.5$§ | $k_{cat,FA} = 0.134 \text{ s}^{-1}$ | $K_{M,FA} = 0.136$ |
| $B \xrightarrow{A^*} B^*$ | $B = 1$ | $A^* = 0$ | $k_{cat,B} = 0.262 \text{ s}^{-1}$ | $K_{M,B} = 0.200$ |
| $B^* \xrightarrow{F_B} B$ | $B^* = 0$ | $F_B = 0.5$§ | $k_{cat,FB} = 0.104 \text{ s}^{-1}$ | $K_{M,FB} = 0.223$ |
| $C \xrightarrow{B^*} C^*$ | $C = 1$ | $B^* = 0$ | $k_{cat,C} = 0.539 \text{ s}^{-1}$ | $K_{M,C} = 2.009$ |
| $C^* \xrightarrow{F_C} C$ | $C^* = 0$ | $F_C = 0.5$§ | $k_{cat,FC} = 0.111 \text{ s}^{-1}$ | $K_{M,FC} = 0.221$ |
| Various | | | $k_{cat,feedback} = 0.277 \text{ s}^{-1}$ | $K_{M,feedback} = 0.539$ |

†Species concentrations are shown in arbitrary units.
‡Rate parameters were optimized so that knockdown and inhibition of *B* yielded the same inhibition of *C** across the full range of *B* perturbation in the linear cascade.
§Deactivating enzymes were kept constant throughout the simulations.

## SUPPLEMENTAL EXPERIMENTAL PROCEDURES

### Michaelis-Menten Model

A three-tiered enzymatic cascade was modeled using Michaelis-Menten kinetics for forward (activation) and reverse (deactivation) reactions. Parameter sets for the model are listed in Table S1. The upstream input ($I^*$) was activated from 0–5 minutes to provide a transient signaling event that could propagate through the enzyme cascade. Reverse deactivation reactions were assumed to be constitutive. The system of three differential equations was solved using the MATLAB ode15s solver with relative tolerance = $10^{-3}$ and absolute tolerance = $10^{-6}$. To compare inhibition profiles (Figure 1F), the cascade output C* was integrated over time then normalized to the uninhibited state. Original code is included in File S1.

For the survey of network architecture, the three-tiered enzymatic cascade was elaborated with 14 single-edge topologies (positive and negative links; feedback, feed-forward, and auto-regulation) and 84 double-edge topologies (paired combinations of the 14 single-edge links ignoring directly incoherent pairs, such as $B \rightarrow B$ plus $B \dashv B$; Figure S3A). Rate parameters were optimized as above to produce a linear inhibition profile of $B$ for both knockdown and inhibition in the linear cascade. Parameter sets for the models are listed in Table S2. Each network topology was individually coded as a system of three ordinary differential equations in MATLAB and simulated for inhibition levels from 0 to 99% in 1% increments as described above. The difference between knockdown and inhibition was calculated for each increment then summed to estimate the area between curves. The area between curves was assigned a negative value if inhibition was more potent than knockdown and a positive value if knockdown was more potent than inhibition (Figure 4A). Parameter sensitivity in the models was estimated by doubling or halving each initial condition or rate constant and rerunning the simulations (Figures S3B–E). Original code is included in File S1.

### Mitogen-Activated Protein Kinase (MAPK) Mass-Action Model

A MAPK model was constructed using mass-action kinetics in MATLAB. The three-tiered Raf–MEK–ERK cascade was extracted from a larger mass-action model of receptor tyrosine kinase signaling (Chen et al., 2009). The extracted model contained twenty-two distinct species and thirty-two rate parameters. Two rate parameters were adjusted in the phosphatase reactions to enable realistic recovery to baseline following upstream activation (File S1). In addition, one reaction was added to allow unphosphorylated MEK to bind ERK at a rate equivalent to the binding rate of phosphorylated MEK (Aoki et al., 2011). This reaction was needed to encode the mechanism of action of U0126 (see below).

ERK $\dashv$ Raf negative feedback was added via a five-site inhibitory phosphorylation pathway consistent with the five Ser-Pro sites on Raf that are directly phosphorylated by ERK (Figure 2B) (Dougherty et al., 2005). Raf species with one or more ERK-catalyzed phosphorylation site were considered unable to interact with MEK or phosphorylated MEK. The feedback rate parameters were derived from an existing ERK-catalyzed feedback reaction within the larger mass-action model (ERK $\dashv$ C:Grb2:Gab1) (Chen et al., 2009). The reversal of hyperphosphorylated Raf was modeled as a phosphatase reaction catalyzed by PP2A(I) using the same rate parameters for the dephosphorylation of active phosphorylated Raf. The concentration of PP2A(I) was increased by 1.5-fold to achieve smooth trajectories in Raf activation in the presence of ERK $\dashv$ Raf feedback. Active ERK was assumed to hyperphosphorylate both the inactive and active forms of Raf, because the sites of activating and inhibitory phosphorylation are distinct. Modeling ERK $\dashv$ Raf feedback created 62 distinct forms of hyper-phosphorylated Raf and 124 additional intermediates (File S1).

For MEK perturbations, knockdown was modeled by scaling the initial concentration of MEK species according to the extent of knockdown. Perturbation with MEKi was modeled as a reversible binding reaction between MEKi and inactive MEK. The binding affinity for the MEKi–MEK interaction was modeled based on experimental studies of the U0126 inhibitor ($K_I$ = 0.041 μM) (Favata et al., 1998). The MEKi-MEK complex was allowed to bind to ERK as described above but was prohibited from binding to Raf. Modeling results (Figure 2) were qualitatively equivalent regardless of whether Raf binding to MEK or Raf catalysis of MEK phosphorylation was prohibited.

To simulate pathway activation in the model, the cascade was initiated by a step increase in GTP loading of the Raf activator Ras (40% of total Ras to RasGTP) for 5 minutes. Thereafter, RasGTP levels were dropped to zero and the model was run for an additional 5 minutes. The system of 212 differential equations was solved using the MATLAB ode15s solver with relative tolerance = $10^{-8}$ and absolute tolerance = $10^{-10}$. MEK perturbations were matched by simulating the cascade without ERK $\dashv$ Raf feedback and matching the MEKi concentration and extent of knockdown that achieved equivalent MEK suppression at the 5-minute endpoint. With matched perturbations,

the cascade was simulated with and without ERK –| Raf feedback. Bis-phosphorylated active (ERK**) was integrated over time and normalized to the uninhibited state for that model, and alternative metrics (peak ERK**, rate of ERK** formation, and ERK** abundance at 5 minutes) were also tested (Figures S1C–E). The difference in integrated ERK** was computed between MEK Knockdown (KD) and MEK Inhibitor (Inh) at 2% increments of MEK perturbation. Original code is included in File S1.

**Cell Culture**
NIH 3T3 cells (ATCC) were cultured according to the provider's recommendations.

**Cell Stimulation and Lysis**
NIH 3T3 cells were plated at 18,000 cells/cm$^2$ for 24 hours, changed to serum free media for 24 hours, pretreated with FR180204 (20 $\mu$M, Sigma) and U0126 (2 $\mu$M, Tocris) for 30 minutes or U0126 alone for one hour and stimulated with PDGF-BB (PeproTech) or 4-hydroxytamoxifen (Sigma) as indicated. Cells were lysed in radioimmunoprecipitation assay buffer (Pierce) supplemented with protease inhibitors.

**Plasmids**
Sequences targeting murine MEK1 and MEK2 were cloned by ligating annealed oligonucleotides (shRNA #1: ccggCCAGATCATCCGGGAGCTGCActgcagTGCAGCTCCCGGATGATCTGGtttttg and aattcaaaaaCCAGATCATCCGGGAGCTGCActgcagTGCAGCTCCCGGATGATCTGG; shRNA #2: ccggGCTGATCCACCTGGAGATCAActgcagTTGATCTCCAGGTGGATCAGCtttttg and aattcaaaaaGCTGATCCACCTGGAGATCAActgcagTTGATCTCCAGGTGGATCAGC; targeting sequence in caps) into pLKO.1 puro or pLKO.1 neo digested with AgeI and EcoRI.
A pre-established control sequence targeting GFP (Sancak et al., 2008) was cloned by ligating annealed oligonucleotides (ccggGCAAGCTGACCCTGAAGTTCATctgcagATGAACTTCAGGGTCAGCTTGCtttttg and aattcaaaaaGCAAGCTGACCCTGAAGTTCATctgcagATGAACTTCAGGGTCAGCTTGC; targeting sequence in caps) into pLKO.1 neo digested with AgeI and EcoRI.
pLKO.1 shGFP puro targeting the same sequence (Orimo et al., 2005) was obtained from Addgene (Plasmid #12273).

For the hormone-responsive, feedback-resistant Raf allele, residues 306–648 of human Raf1 were PCR amplified from a feedback-resistant Raf1-6A construct (Dougherty et al., 2005) obtained from Deborah Morrison. An N-terminal HA tag was appended by PCR to yield HA-ΔRaf1(S642A), which was digested with BamHI and EcoRI and ligated into pBabe ΔMEKK3:ER* puro (Garner et al., 2002) from Simon Cook that had been similarly digested to release the ΔMEKK3 fragment. Five residues upstream of the EcoRI ligation site were inserted by site-directed mutagenesis (QuikChange XLII, Stratagene) to move the ER* hormone-binding domain in frame with HA-ΔRaf1(S642A) and yield pBabe HA-ΔRaf1(S642A):ER* puro. All plasmids were verified by restriction digest and sequencing and have been deposited with Addgene.

**Viral Transduction**
Lentiviruses and retroviruses were packaged and transduced into NIH 3T3 cells as described previously (Wang et al., 2011). For the shMEK1/2 line with 80% knockdown (Figure 3), cells were transduced once overnight with a 1:2 dilution of packaged virus to ensure saturated binding of the available amphotropic viral receptors. For the HA-ΔRaf1(S642A):ER* line, cells were transduced once overnight with a 1:2 dilution of packaged virus. For the shMEK1/2 v2 line with 97% knockdown (Figure S2G), cells were transduced twice overnight with a 1:2 dilution of packaged virus and eight hours of recovery in between. shGFP control lines were established according to the same transduction protocol as the matched shMEK1/2 line. Stably transduced NIH 3T3 cells were selected with puromycin (1 μg/ml) until control plates had cleared. After stable selection in puromycin, the HA-ΔRaf1(S642A):ER* line was subsequently transduced twice overnight with a 1:2 dilution of shMEK1/2 or shGFP and then selected with puromycin (1 μg/ml) plus G418 (600 μg/ml) until control plates had cleared.

**Immunoblotting**
Equal amounts of clarified lysates (10 μg) were separated by SDS-polyacrylamide gel electrophoresis and transferred onto polyvinylidene difluoride membranes (Millipore or BioRad). Membranes were blocked for 1 hour in 0.5× blocking solution (LI-COR). Membranes were incubated overnight with primary antibodies recognizing the following proteins or epitopes: phosphorylated c-Raf (Ser289/296/301, Cell Signaling Technology, #9431; 1:1000), c-Raf (Santa Cruz Biotechnology, #sc-133; 1:1000), phosphorylated MEK1/2 (Ser217/221, Cell Signaling

Technology, #9121; 1:1000), phosphorylated ERK1/2 (Thr202/Tyr204, Cell Signaling Technology, #4370; 1:1000), MEK1/2 (Cell Signaling Technology, #4694; 1:1000), ERK1/2 (Cell Signaling Technology, #4696; 1:1000), HA (Roche, #11867423001; 1:2000), β-actin (Cell Signaling Technology, #3700; 1:5000), tubulin (Abcam, #ab4074; 1:20,000), Hsp90 (Santa Cruz Biotechnology, #sc-7947; 1:2000), and vinculin (Millipore, #05-386; 1:20,000). Subsequently, membranes were incubated with secondary IRDye-conjugated antibodies (LI-COR; 1:20,000). Protein bands were detected by an Odyssey infrared scanner (LI-COR). Densitometry of bands was performed in ImageJ as described (Janes, 2015).

**Immunofluorescence**

No. 1.5 coverslips were treated with poly-D-lysine hydrobromide (Sigma) before cell plating. Immunofluorescence was performed as described previously (Wang et al., 2011) with a primary antibody against phosphorylated Rb (Ser807/811, Cell Signaling Technology; 1:1000).

**SUPPLEMENTAL REFERENCES**

Garner, A.P., Weston, C.R., Todd, D.E., Balmanno, K., and Cook, S.J. (2002). Delta MEKK3:ER* activation induces a p38 alpha/beta 2-dependent cell cycle arrest at the G2 checkpoint. Oncogene *21*, 8089-8104.

Orimo, A., Gupta, P.B., Sgroi, D.C., Arenzana-Seisdedos, F., Delaunay, T., Naeem, R., Carey, V.J., Richardson, A.L., and Weinberg, R.A. (2005). Stromal fibroblasts present in invasive human breast carcinomas promote tumor growth and angiogenesis through elevated SDF-1/CXCL12 secretion. Cell *121*, 335-348.

Sancak, Y., Peterson, T.R., Shaul, Y.D., Lindquist, R.A., Thoreen, C.C., Bar-Peled, L., and Sabatini, D.M. (2008). The Rag GTPases bind raptor and mediate amino acid signaling to mTORC1. Science *320*, 1496-1501.